J. Appl. Comput. Mech., 5(5) (2019) 964-975
DOI: 10.22055/JACM.2019.27938.1443

ISSN: 2383-4536
jacm.scu.ac.ir

M&MoCS

Shahid Chamran University of Ahvaz

Journal of Applied and Computational Mechanics

Research Paper

Numerical and Analytical Approach for Film Condensation on Different Forms of Surfaces

Ammar Kazemi Jouybari[1], Arash Mirabdolah Lavasani[2]

[1] Department of Mechanical Engineering, Islamic Azad University, Central Tehran Branch, Tehran, Iran, ammar.kazemi.eng@iauctb.ac.ir,

[2] Department of Mechanical Engineering, Islamic Azad University, Central Tehran Branch, Tehran, Iran, arashlavasani@iauctb.ac.ir

Received December 18 2018; Revised February 18 2019; Accepted for publication March 06 2019.
Corresponding author: A.K. Jouybari, ammar.kazemi.eng@iauctb.ac.ir

Abstract. This paper tries to achieve a solution for problems that concern condensation around a flat plate, circular and elliptical tube in by numerical and analytical methods. Also, it calculates entropy production rates. At first, a problem was solved with mesh dynamic and rational assumptions; next it was compared with the numerical solution that the result had acceptable errors. An additional supporting relation is applied based on the characteristic of the condensation phenomenon for condensing elements. As it is shown here, due to higher rates of heat transfer for elliptical tubes, they have more entropy production rates, in comparison to circular ones. Findings showed that the two methods were efficient. Furthermore, analytical methods can be used to optimize the problem and reduce the entropy production rate.

Keywords: Entropy rate, Analytical solution, Numerical solution, Condensation.

1. Introduction

Energy saving and increasing productivity depend on designing thermal and thermodynamic transfer processes which can prevent energy losses. Exergy and entropy production determine the efficiency of a system. High entropy production rates indicate inefficiency and reducing it in the thermal systems can be a design goal.

There are many studies that investigate the ways of reducing entropy in a process. Most of which have considered the process systems that include multiple components [1-2]. Different studies like [3], [4], and [5] have worked on increasing heat transfer of condensation. These studies evaluated the surfaces with a fin of a cylinder with an elliptical cross-section. They pointed out that the gravitational impact of using elliptical tubes leads to an improvement in heat transfer. In fact, increasing the heat transfer along with increasing thermal flux leads to higher friction coefficient and ultimately increases the pump power consumption.

This section reviews some studies in the fields of heat transfer with reducing entropy production and improving the performance of the thermal process in order to find a suitable point to increase heat transfer and reduce the friction coefficient. Bejan [6] is one of the pioneers in minimizing of entropy production in heat transfer analysis. He propounded a thermodynamical optimization to achieve higher pump power by increasing friction coefficient and dimensionless differential temperature along with decreasing entropy production rate.

Sahin [7] studied the effect of viscosity related to temperature on entropy production rate in cylindrical sections and evaluated pump power for effective heat transfer. Adeyinka and Naterer [8] examined the importance of entropy production in film condensation on a cylinder. Lin et al. [9] studied the first analysis of a saturated vapor flow from the standpoint of the second law of thermodynamics. They calculated an optimal Reynolds number in horizontal tubes, in which the entropy production is at the minimum level. Dung and Yang [10] developed their study on an isothermal tube based on entropy

Published online: June 14 2019

production. Results showed that the entropy production is a useful parameter to optimize a two-phase system. Li and Yang [11] investigated an elliptical cylinder with film condensation exposed to a free convection stream by evaluating entropy production rate.

Theoretical solutions possess many assumptions and limits, so they are not practical for many industrial applications. However, in this paper, the suggested numerical model for two-dimensional condensation is elaborated. Although numerical solutions are time-consuming, they can solve more thorough problems. As an example, in the case of condensation around the tubes, the numerical solutions cover boundaries with suction and changing temperature distributions as well as rotating tubes in all conditions. Besides, the transient state can be modelled in numerical solutions, whereas in theoretical solutions, we can just consider steady state problems. In this paper, Field diagrams for both theoretical and numerical methods compared with each other. As it will show in the following, the two methods were efficient.

2. Statement of Relations

As can be seen from Fig. 1, the elements of mass and energy condensation are shown in the schematic. In this paper, it is tried to use a scalar field quantity to determine the boundary shape. This quantity is defined in the center of each element as follows:

$$\mathrm{q} = \frac{\mathrm{h}}{\mathrm{dy}} - \mathrm{N}, \tag{1}$$

where h is the boundary height an N is the number of available elements in the liquid phase in each determined X (longitudinal) and $\mathrm{q} = (\mathrm{Volume}_{\text{liquid int the Element}}) / (\mathrm{Volume}_{\text{Total mass of Element}})$ when phase is changing, Auxiliary equation is as:

$$\frac{\partial \mathrm{T}}{\partial \mathrm{t}} = 0 \quad \mathrm{q} <= 1, \tag{2}$$

The equation changes as a result of energy consumption to change temperature in the liquid region as:

$$\frac{\partial \mathrm{q}}{\partial \mathrm{t}} = 0 \quad \mathrm{q} = 1, \tag{3}$$

Meshing should be carried on in a variable form, because fixed meshing takes a very long time due to excessive calculations. The value of temperature and pressure equals with saturated values in the gas element. Because of the small directional conductivity of vapor conduction and the absence of convection, the vapor temperature is equal to saturated temperature, even if in reality, the temperature of vapor is slightly higher than the saturation temperature. So, this is an efficient assumption in many industrial applications. In the solution procedure, as soon as the element is filled in each X (q=1), the value of N increases as much as 1 and meshing increases with growing boundary in this way.

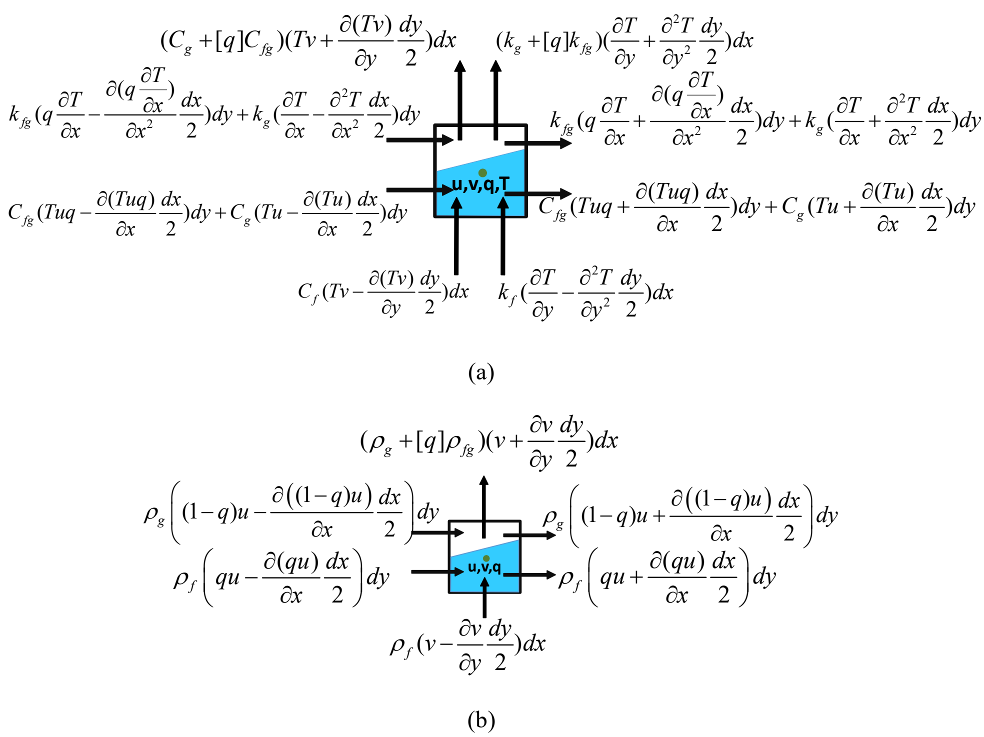

Fig. 1. The relevant elements, (a) mass balance (b) energy balance

There are two continuity equations; due to the fact that the problem is a two-phase problem including the liquid phase and the whole element. In addition to the input and output quantities, some of the vapor is converted to the liquid in the element of liquid phase. The amount of this mass conversion is obtained from the energy equation. According to Fig. 1 that can show mass balance:

$$\begin{gathered}\sum m_{in}-\sum m_{out}=\frac{\partial m_{C.V}}{\partial t},\\ \Rightarrow -\rho_{fg}\frac{\partial(qu)}{\partial x}dxdy-\rho_g\frac{\partial u}{\partial x}dxdy+\rho_{fg}(1-[q])vdx-(\rho_g+\rho_f+[q]\rho_{fg})\frac{\partial v}{\partial y}\frac{dy}{2}dx=\frac{\partial m_{C.V}}{\partial t},\end{gathered} \tag{4}$$

As noted in the q definition, $\partial m_{C.V}/\partial t=(\rho_{fg}\partial q/\partial t)\,dxdy$ consequently. Considering the continuity law:

$$\begin{gathered}\sum mf_{in}-\sum mf_{out}+\dot{m}_{Condensation}dxdy=\frac{\partial mf_{C.V}}{\partial t},\\ \Rightarrow -\rho_f\frac{\partial(qu)}{\partial x}+\rho_f(1-[q])\frac{v}{dy}-\tfrac{1}{2}(\rho_f+[q]\rho_f)\frac{\partial v}{\partial y}+\dot{m}_{Condensation}=\rho_f\frac{\partial q}{\partial t},\end{gathered} \tag{5}$$

As can be seen from Fig. 1a, the temperatures are very low which radiation heat transfer can be neglected. So, the only conductive heat transfer and displacement is studied in this problem. The conductive heat transfer is calculated from the Fourier formula which has shown their values in four boundaries of the element in Fig. 1b. For the two-phase boundaries, these values are averaged by using q field.
In the following, the amount of output and input enthalpies should be studied in the liquid phase and saturation region. Enthalpy is considered only as a function of temperature and here we used thermal capacity for liquid and vapor phases. Now, to investigate the rate of condensation, it is enough to calculate the balance of input and output enthalpy and transmitted conduction heat energy. So:

$$\Sigma Q_{in}-\Sigma Q_{out}=A+B+C+D, \tag{6a}$$

where

$$\begin{gathered}A=C_{fg}\left(uq-\frac{\partial(uq)}{\partial x}\frac{dx}{2}\right)\left(-\frac{\partial T}{\partial x}\frac{dx}{2}\right)dy+C_g\left(u-\frac{\partial u}{\partial x}\frac{dx}{2}\right)\left(-\frac{\partial T}{\partial x}\frac{dx}{2}\right)dy+k_{fg}\left(q\frac{\partial T}{\partial x}-\frac{\partial(q\frac{\partial T}{\partial x})}{\partial x}\frac{dx}{2}\right)dy+k_g\left(\frac{\partial T}{\partial x}-\frac{\partial^2 T}{\partial x^2}\frac{dx}{2}\right)dy,\\ B=-\left\{C_{fg}\left(uq+\frac{\partial(uq)}{\partial x}\frac{dx}{2}\right)\left(\frac{\partial T}{\partial x}\frac{dx}{2}\right)dy+C_g\left(u+\frac{\partial u}{\partial x}\frac{dx}{2}\right)\left(\frac{\partial T}{\partial x}\frac{dx}{2}\right)dy+k_{fg}\left(q\frac{\partial T}{\partial x}+\frac{\partial(q\frac{\partial T}{\partial x})}{\partial x^2}\frac{dx}{2}\right)dy+k_g\left(\frac{\partial T}{\partial x}+\frac{\partial^2 T}{\partial x^2}\frac{dx}{2}\right)dy\right\},\\ C=C_f\left(v-\frac{\partial(v)}{\partial y}\frac{dy}{2}\right)\left(-\frac{\partial T}{\partial y}\frac{dy}{2}\right)dx+k_f\left(\frac{\partial T}{\partial y}-\frac{\partial^2 T}{\partial y^2}\frac{dy}{2}\right)dx,\\ D=-\left\{\left(C_g+[q]*C_{fg}\right)\left(v+\frac{\partial v}{\partial y}\frac{dy}{2}\right)\left(\frac{\partial T}{\partial y}\frac{dy}{2}\right)dx+\left(k_g+[q]*k_{fg}\right)\left(\frac{\partial T}{\partial y}+\frac{\partial^2 T}{\partial y^2}\frac{dy}{2}\right)dx\right\},\end{gathered} \tag{6b}$$

By simplifying, the amount of transmitted energy can be obtained as follows:

$$\begin{gathered}\sum Q_{in}-\sum Q_{out}=\left\{-(C_{fg}q+C_g)u\frac{\partial T}{\partial x}+k_{fg}\,\partial(q\frac{\partial T}{\partial x})\Big/\partial x+k_g\frac{\partial^2 T}{\partial x^2}\right\}+\\ \left\{-\tfrac{1}{2}(C_g+C_f+[q]C_{fg})v\frac{\partial T}{\partial y}+k_{fg}(1-[q])\left(\frac{\partial T}{\partial y}\right)\Big/dy+\tfrac{1}{2}\left(k_g+k_g+[q]k_{fg}\frac{\partial^2 T}{\partial y^2}\right)\right\},\end{gathered} \tag{7}$$

Next, energy equations are extended by auxiliary equations and the related friction relations. It was noted that how auxiliary equations can be obtained from the fact that the temperature remains constant at the phase change and that the volume ratio is constant in the liquid section. This equation is directly used to calculate thermal energy variations. So:

$$\begin{gathered}\frac{\partial Q_{C.V}}{\partial t}=Q_{Viscous-Heat}-Ldxdy\dot{m}_{Condensation}, \qquad T=T_{Sat}\\ \frac{\partial Q_{C.V}}{\partial t}=Q_{Viscous-Heat}+(C_g+qC_{fg})dxdy\frac{\partial T}{\partial t}, \qquad T\neq T_{Sat}\end{gathered} \tag{8}$$

where L is the latent heat of evaporation and C is the heat capacity. In the following, the work done by frictional force is calculated, and it can be expressed as:

$$Q_1 = F_y^- v^- = \left\{ \mu_{fg} \left(q\frac{\partial v}{\partial x} - \frac{\partial\left(q\frac{\partial v}{\partial x}\right)}{\partial x}\frac{dx}{2} \right) + \mu_g \left(\frac{\partial v}{\partial x} - \frac{\partial^2 v}{\partial x^2}\frac{dx}{2} \right) \right\} .dx \left(v - \frac{\partial v}{\partial x}\frac{dx}{2} \right), \tag{9}$$

$$Q_2 = F_y^+ v^+ = -\left\{ \mu_{fg} \left(q\frac{\partial v}{\partial x} + \frac{\partial\left(q\frac{\partial v}{\partial x}\right)}{\partial x}\frac{dx}{2} \right) + \mu_g \left(\frac{\partial v}{\partial x} + \frac{\partial^2 v}{\partial x^2}\frac{dx}{2} \right) \right\} .dx \left(v + \frac{\partial v}{\partial x}\frac{dx}{2} \right), \tag{10}$$

$$Q_3 = F_x^- u^- = \mu_f \left(\frac{\partial u}{\partial y} - \frac{\partial^2 u}{\partial y^2}\frac{dy}{2} \right) .dx \left(u - \frac{\partial u}{\partial y}\frac{dy}{2} \right), \tag{11}$$

$$Q_4 = F_x^+ u^+ = -\left(\mu_g + [q]\mu_{fg}\right) \left(\frac{\partial u}{\partial y} + \frac{\partial^2 u}{\partial y^2}\frac{dy}{2} \right) .dx \left(u + \frac{\partial u}{\partial y}\frac{dy}{2} \right), \tag{12}$$

Therefore, energy equation can be written for the element with respect to the total lost work as the following:

$$\begin{cases} \text{if } T = T_{sat} \text{ then } L\dot{m}_{condensation} \\ \text{if } T \neq T_{sat} \text{ then } \left(C_{fg}q + C_g\right)\dfrac{\partial T}{\partial t} \end{cases} = \left\{ -\left(C_{fg}q + C_g\right)u\frac{\partial T}{\partial x} + k_{fg}\,\partial\left(q\frac{\partial T}{\partial x}\right)\Big/\partial x + k_g\frac{\partial^2 T}{\partial x^2} \right\} + \tag{13}$$
$$\left\{ -\tfrac{1}{2}\left(C_g + C_f + [q]C_{fg}\right)v\frac{\partial T}{\partial y} + k_{fg}\left(1-[q]\right)\left(\frac{\partial T}{\partial y}\right)\Big/dy + \tfrac{1}{2}\left(k_g + k_g + [q]k_{fg}\frac{\partial^2 T}{\partial y^2} \right) \right\},$$

As shown in the above equation, there is solitary in y direction, but if q = 1 there is not singularity. The total input and output of momentum in tangential direction are obtained as follows:

$$\sum P_{Xin} - \sum P_{Xout} + F_x = -\rho_{fg}\frac{\partial\left(qu^2\right)}{\partial x} - \rho_g\frac{\partial\left(u^2\right)}{\partial x} + \rho_{fg}\left(1-[q]\right)u\frac{v}{dy} - \left(\rho_g + [q]\rho_{fg} + \rho_f\right)\frac{\partial(uv)}{\partial y} - \tag{14}$$
$$\frac{\partial P}{\partial x} + \left(\rho_g + q\rho_{fg}\right)g_x + \left(1-[q]\right)\mu_{fg}\left(\frac{\partial u}{\partial y}\right)\Big/dy - \left(\mu_g + [q]\mu_{fg} + \mu_f\right)\frac{\partial^2 u}{\partial y^2},$$

After calculating the momentum of control volume:

$$-\rho_{fg}\frac{\partial\left(qu^2\right)}{\partial x} - \rho_g\frac{\partial\left(u^2\right)}{\partial x} + \rho_{fg}\left(1-[q]\right)u\frac{v}{dy} - \left(\rho_g + [q]\rho_{fg} + \rho_f\right)\frac{\partial(uv)}{\partial y} + \left(\rho_g + q\rho_{fg}\right)g_x - \frac{\partial P}{\partial x} + \tag{15}$$
$$\left(1-[q]\right)\mu_{fg}\frac{\left(\frac{\partial u}{\partial y}\right)}{dy} - \left(\mu_g + [q]\mu_{fg} + \mu_f\right)\frac{\partial^2 u}{\partial y^2} = \left(\rho_g + q\rho_{fg}\right)\frac{\partial u}{\partial t} + \rho_{fg}u\frac{\partial q}{\partial t},$$

Considering the output and input momentum in tangential and vertical directions for the element, the ultimate equation can be written as follows:

$$-\rho_{fg}\frac{\partial(quv)}{\partial x} - \rho_g\frac{\partial(uv)}{\partial x} + \rho_{fg}\left(1-[q]\right)v\frac{v}{dy} - \left(\rho_g + [q]\rho_{fg} + \rho_f\right)\frac{\partial\left(v^2\right)}{\partial y} - \frac{\partial P}{\partial y} + \left(\rho_g + q\rho_{fg}\right)g_y + \mu_{fg}\left(\frac{\partial\left(q\frac{\partial v}{\partial x}\right)}{\partial x} \right) + \mu_g\left(\frac{\partial^2 v}{\partial x^2}\right) \tag{16}$$
$$= \left(\rho_g + q\rho_{fg}\right)\frac{\partial v}{\partial t} + \rho_{fg}v\frac{\partial q}{\partial t},$$

Now, these equations must be converted into a desired form which is necessary for numerical solution. That is to say, the sequence of applying these equations is determined and the equations must be in the form in which the corresponding terms are obtained at each stage.

First, energy equation should be solved to calculate condensing mass in the boundary region and the temperature rise in the liquid region. Equation (13) can be used as follows:

$$\begin{aligned}\frac{\partial T}{\partial t}=\frac{1}{C_f}&\left(\left\{-\left(C_{fg}q+C_g\right)u\frac{\partial T}{\partial x}+k_{fg}\,\partial\left(q\frac{\partial T}{\partial x}\right)\Big/\partial x+k_g\frac{\partial^2 T}{\partial x^2}\right\}+\right.\\ &\left.\left\{-\tfrac{1}{2}\left(C_g+C_f+[q]C_{fg}\right)v\frac{\partial T}{\partial y}+k_{fg}\left(1-[q]\right)\left(\frac{\partial T}{\partial y}\right)\Big/dy\right\}+\tfrac{1}{2}\left\{k_g+k_g+[q]k_{fg}\frac{\partial^2 T}{\partial y^2}\right\}\right).[q],\end{aligned} \tag{17}$$

$$\begin{aligned}\dot{m}_{condensation}=\frac{1}{h_{fg}}&\left(\left\{-\left(C_{fg}q+C_g\right)u\frac{\partial T}{\partial x}+k_{fg}\,\partial\left(q\frac{\partial T}{\partial x}\right)\Big/\partial x+k_g\frac{\partial^2 T}{\partial x^2}\right\}+\right.\\ &\left.\left\{-\tfrac{1}{2}\left(C_g+C_f+[q]C_{fg}\right)v\frac{\partial T}{\partial y}+k_{fg}\left(1-[q]\right)\left(\frac{\partial T}{\partial y}\right)\Big/dy\right\}+\tfrac{1}{2}\left\{k_g+k_g+[q]k_{fg}\frac{\partial^2 T}{\partial y^2}\right\}\right).\left(1-[q]\right),\end{aligned} \tag{18}$$

Now, the growth rate of q can be obtained from the equation of mass balance in the liquid phase, because the amount of $\dot{m}_{Condensation}$ is known:

$$\frac{\partial q}{\partial t}=-\frac{\partial(qu)}{\partial x}+\left(1-[q]\right)\frac{v}{dy}-\tfrac{1}{2}\left(1+[q]\right)\frac{\partial v}{\partial y}+\frac{\dot{m}_{Condensation}}{\rho_f}, \tag{19}$$

There are some presented methods to solve above coupling in computational fluid dynamics (CFD) for single-phase fields. By separation of the mass balance equation in the liquid phase and the general state, and knowing the growth rate q from mass balance of the liquid phase, we can generalize these methods to this problem. First, explicit terms of momentum balance, u^* and v^* are obtained as follows:

$$\begin{aligned}u^*=&\left(-\rho_{fg}\frac{\partial\left(qu^2\right)}{\partial x}-\rho_g\frac{\partial\left(u^2\right)}{\partial x}+\rho_{fg}\left(1-[q]\right)u\frac{v}{dy}-\left(\rho_g+[q]\rho_{fg}+\rho_f\right)\frac{\partial(uv)}{\partial y}+\left(\rho_g+q\rho_{fg}\right)g_x\right.\\ &\left.+\left(1-[q]\right)\mu_{fg}\left(\frac{\partial u}{\partial y}\right)\Big/dy-\left(\mu_g+[q]\mu_{fg}+\mu_f\right)\frac{\partial^2 u}{\partial y^2}-\rho_{fg}u\frac{\partial q}{\partial t}\right),\end{aligned} \tag{20}$$

and

$$\begin{aligned}v^*=&\left(-\rho_{fg}\frac{\partial(quv)}{\partial x}-\rho_g\frac{\partial(uv)}{\partial x}-\left(\rho_g+[q]\rho_{fg}+\rho_f\right)\frac{\partial\left(v^2\right)}{\partial y}+\mu_g\left(\frac{\partial^2 v}{\partial x^2}\right)+\rho_{fg}\left(1-[q]\right)v\frac{v}{dy}+\left(\rho_g+q\rho_{fg}\right)g_y+\right.\\ &\left.\mu_{fg}\left(\partial\left(q\frac{\partial v}{\partial x}\right)\Big/\partial x\right)-\rho_{fg}v\frac{\partial q}{\partial t}\right),\end{aligned} \tag{21}$$

In order for more details about how to use them, one can refer to [11]. By replacing the pressure field u^* and v^* in relations, (20) and (21), the velocity field is obtained at the next moment. The rate of volumetric entropy production is calculated by the numerical integration of the velocity field and temperature from the following formula:

$$\dot{S}'''_{gen}=\frac{k}{T^2}\left[\left(\frac{\partial T}{\partial x}\right)^2+\left(\frac{\partial T}{\partial y}\right)^2\right]+\frac{\mu}{T}\left\{2\left[\left(\frac{\partial v_x}{\partial x}\right)^2+\left(\frac{\partial v_y}{\partial y}\right)^2\right]+\left[\left(\frac{\partial v_x}{\partial y}+\frac{\partial v_y}{\partial x}\right)^2\right]\right\}, \tag{22}$$

3. Discretization of Equations

In this section, the obtained equations from FDM method are discretized. The square element arrangement which has been used here is shown in Fig. 2.

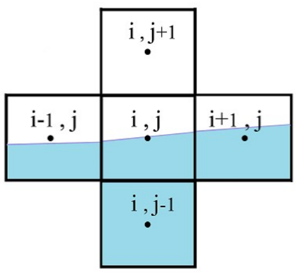

Fig. 2. Elemental Arrangement for Calculating Order Derivative

The orders of derivative are calculated as follows:

$$\begin{aligned}&\frac{\partial f}{\partial x}=\frac{f_{i+1,j}-f_{i-1,j}}{2dx},\\&\frac{\partial^2 f}{\partial x^2}=\frac{f_{i+1,j}+f_{i-1,j}-2f_{i,j}}{dx^2},\\&\frac{\partial f}{\partial y}=\frac{f_{i,j+1}-f_{i,j-1}}{2dy},\\&\frac{\partial^2 f}{\partial y^2}=\frac{f_{i,j+1}+f_{i,j-1}-2f_{i,j}}{dy^2},\end{aligned}\tag{23}$$

Doing the above-mentioned calculations for obtained equations for the element, the discretized equations are acquired. The results are not presented here due to being detailed. But discretized equation of mass balance in the liquid phase is as follows (discretized by explicit solution):

$$q_{i,j}^{k+1}=q_{i,j}^{k}+\left(\frac{q_{i+1,j}{}^{k}u_{i+1,j}{}^{k}-q_{i-1,j}{}^{k}u_{i-1,j}{}^{k}}{2\Delta x}\right)\Delta t+\left(\left(1-[q_{i,j}{}^{k}]\right)\frac{v_{i,j}{}^{k}}{\Delta y}-\frac{\left(1+\left[q_{i,j}{}^{k}\right]\right)}{2}\left(\frac{v_{i,j+1}{}^{k}-v_{i,j-1}{}^{k}}{2\Delta y}\right)\right)\Delta t,\tag{24}$$

4. Investigation of Boundary Conditions and How to Apply Them

Boundary conditions are quite clear in the problem of y-direction. Vertical velocity is zero at the wall if there is no suction. Also, the tangential velocity is zero if the tube does not rotate. Temperature is equal to the temperature of the wall.

At the boundary of condensation, the temperature is equal to the temperature of saturated vapor. Vertical velocity is almost zero if the wall does not have suction. But the boundary condition related to tangential direction depends on shear stress at the boundary of condensation. If the examined fluid is a viscous fluid, friction at the boundary is important and it should be calculated in some way. But if the considered fluid has a low viscosity (like water), shear stress can be considered equal to zero. The boundary conditions in X-direction depend on the geometric aspect of the problem. When X=0, the height of boundary of condensation is zero and it means that the starting point in flat plate acts as thermal insulation. In the case of velocities, it can also be considered as an insulating force. Thus, for the flat plate, we have:

$$x=0:\qquad \frac{\partial^2 u}{\partial x^2}=0;\ \frac{\partial^2 v}{\partial x^2}=0;\ \frac{\partial T}{\partial x}=0,\tag{25}$$

By taking advantage of the symmetry in boundary conditions in tangential direction for circular cross-sections, we can consider the model as half of the actual perimeter. As it is known, the geometric conditions are always symmetric in the tubes. If the environmental conditions are symmetric, the half of pipe can be solved and it can be generalized to the other one. In this case, all terms of local rates for temperature and velocities are zero in the direction of X.

If the ambient conditions are not symmetric, the ambiguity can be resolved depending on the alternative conditions. Virtual layers as a usual method are used to apply the boundary conditions. These layers get some quantities in each moment, so that boundary conditions are satisfied. It is obvious that in the case of pressure, singularity of the equations of boundary elements should be resolved without taking any amount for pressure.

5. Determining the Solution Algorithm

Functions can be defined considering the discretized equations for calculating quantities in equation (23). Consequently, the field values of the above quantities are calculated at the first. From equations 16 to 20:

$$\begin{aligned}&T_{i,j}{}^{k+1}=F_{Tem}\left(T_{:,:}{}^{k},u_{:,:}{}^{k},v_{:,:}{}^{k},q_{:,:}{}^{k}\right),\\&q_{i,j}{}^{k+1}=F_{q}\left(T_{:,:}{}^{k},u_{:,:}{}^{k},v_{:,:}{}^{k},q_{:,:}{}^{k}\right),\\&u_{i,j}{}^{*}=F_{u^*}\left(u_{:,:}{}^{k},v_{:,:}{}^{k},q_{:,:}{}^{k}\right),\\&v_{i,j}{}^{*}=F_{v^*}\left(u_{:,:}{}^{k},v_{:,:}{}^{k},q_{:,:}{}^{k}\right),\end{aligned}\tag{26}$$

Subsequently, the field value of above quantities is calculated by using above formulas. About the subject of pressure and velocity coupling, by replacing the amount of velocity in the next moment in the relation of total mass balance, the following relation between the pressure and the frictional velocities can be obtained.

$$A_{MN\times MN}\left(q_{:,:}{}^{k+1}\right)\left(P_{:,:}{}^{k+1}\right)_{MN\times 1}=B\left(q_{:,:}{}^{k+1},u_{:,:}{}^{*},v_{:,:}{}^{*}\right)_{MN\times 1},\tag{27}$$

Therefore, a function that calculates Matrix A and Vector B can now be written. And then pressure field can be determined in the next moment:

$$\begin{aligned} A\left(q_{:,:}^{k+1}\right)_{MN\times MN} &= F_A\left(q_{:,:}^{k+1}, MN\right), \\ B\left(q_{:,:}^{k+1}\right)_{MN\times MN} &= F_B\left(q_{:,:}^{k+1}, u_{:,:}^{*}, v_{:,:}^{*}, MN\right), \end{aligned} \tag{28}$$

As the pressure field is obtained in the next moment, the velocity field of the next moment is also calculated according to Equations (20) and (21). Therefore, it is possible to construct the following functions according to these relations. The solving algorithm is completely illustrated in Fig. 3. Due to the ability of Matlab Software in making Cell, running
The following algorithm is proper in this software. Moreover, because the matrices get smaller, the program runs faster. Respectively from equations 19 and 20:

$$\begin{aligned} u_{:,:}^{k+1} &= F_u\left(u_{:,:}^{*}, P_{:,:}^{k+1}\right), \\ v_{:,:}^{k+1} &= F_v\left(v_{:,:}^{*}, P_{:,:}^{k+1}\right), \end{aligned} \tag{29}$$

6. Investigating the Generality of Equations and Concluding Remarks

In this section, the equations are converted into familiar forms to ensure the accuracy of the equations for the verification purposes. This verification can be seen in Table 1. As stated in the auxiliary equations, in the liquid phase we have $dq/dt = 0$. If we put q = 1 in equation (5), we will have a continuous equation which is continuous relation in the incompressible fluid in Tabel 1. Now, if the above quantities are put in energy balance relation, equation 13 will become the usual form of thermal energy for liquids. There are some unusual terms in the momentum equation that is obtained by putting q = 1. It implies that the obtained equation depends on defined neighborhood dimensions. In other words, these equations are satisfied with an element with certain dimensions. Now, this question comes to the fore: why these equations of elements depend on neighborhood dimensions? The answer is that in general (0 < q < 1), the upward interaction between the element and environment is different from downward interaction.

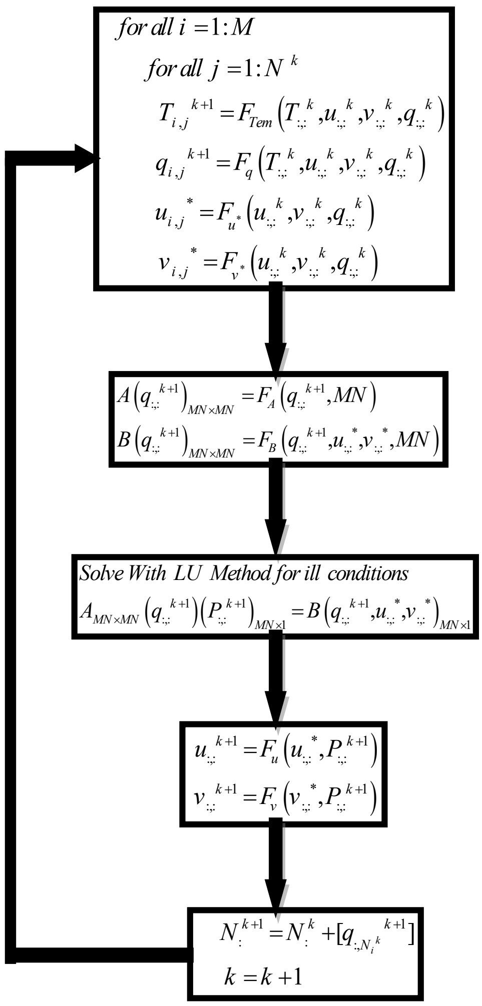

Fig. 3. Numerical solution's algorithm

7. Elaborating the Results

In this section, the result of the numerical model is compared with the analytical solution. Furthermore, the obtained field diagrams are compared with each other. The results showed that two methods are efficient.
Frictional losses are negligible for water. Frictional entropy and dimensionless number φ cannot be plotted because their dimensions are in the range of error tolerances and they are negligible compared with the thermal entropy.

Table 1. Verification of extended equations

Relation	Assumptions	Verification of equations
Equation 4	$dq/dt=0,\ q=1$	$\nabla.\vec{V}=0$
Equation 12	$q=1$	$C_f\frac{\partial T}{\partial t}=\left\{-C_f u\frac{\partial T}{\partial x}+k_f\frac{\partial^2 T}{\partial x^2}\right\}+\left\{-C_f v\frac{\partial T}{\partial y}+k_f\frac{\partial^2 T}{\partial y^2}\right\}$
Equation 15 (Tangential Direction)	$q=1$	$-\rho_f\frac{\partial(u^2)}{\partial x}-\rho_f\frac{\partial(uv)}{\partial y}+\rho_f g_x-\frac{\partial P}{\partial x}-\mu_f\frac{\partial^2 u}{\partial y^2}=\rho_f\frac{\partial u}{\partial t}$
Equation 15 (Vertical Direction)	$q=1$	$-\rho_f\frac{\partial(uv)}{\partial x}-\rho_f\frac{\partial(v^2)}{\partial y}+\rho_f g_y-\frac{\partial P}{\partial y}-\mu_f\frac{\partial^2 v}{\partial x^2}=\rho_f\frac{\partial v}{\partial t}$

The verification of numerical and analytical methods has been presented to boundary conditions and different models. As shown in Fig. 4, models consisted of the vertical flat plate; circle and different shapes of the ellipse are presented according to the constant temperature of boundary conditions. It can be seen that the thickness of the condensation layer increases with the increasing distance from the origin.

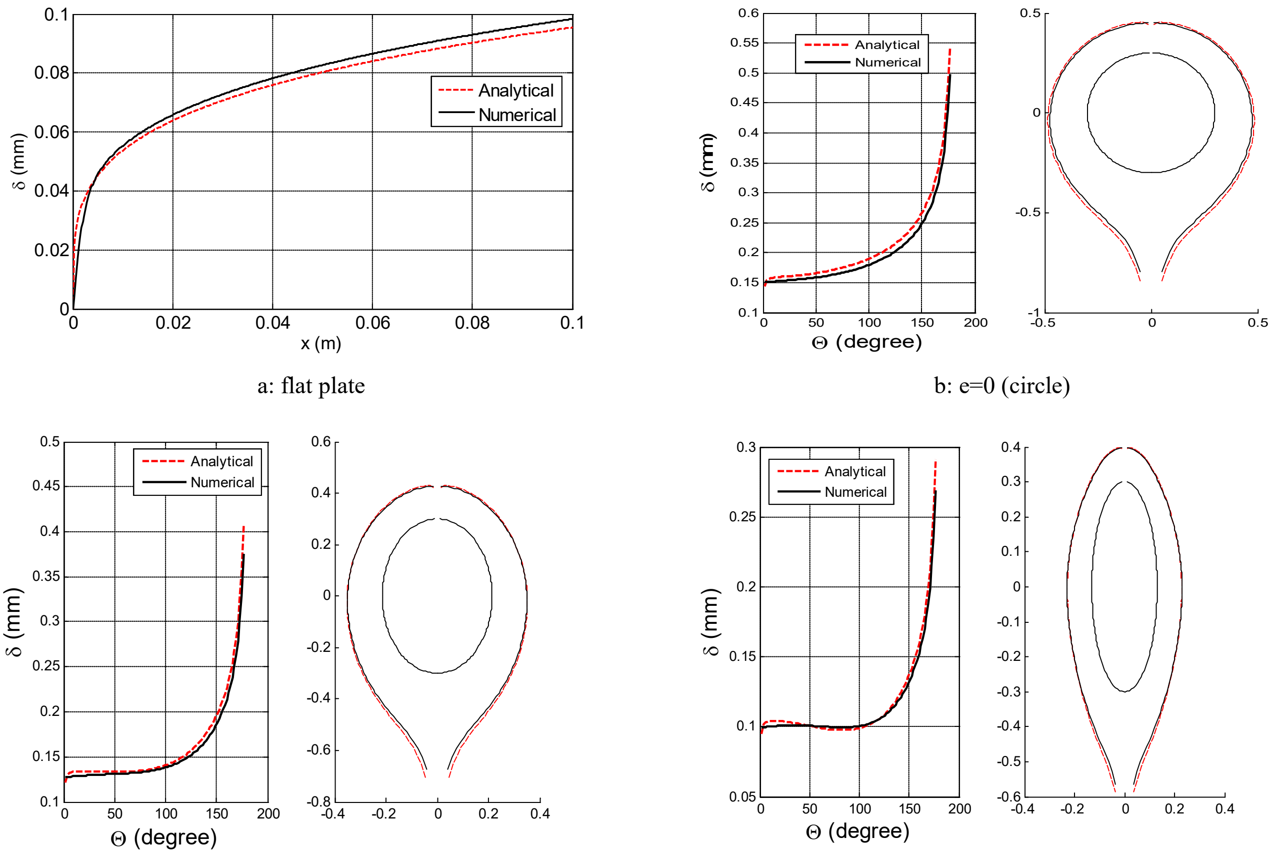

a: flat plate b: e=0 (circle)

c: e=0.7 d: e=0.9

Fig. 4. Condensation Boundary Position for Different States with Constant Temperature Boundary Condition

Also, the problem is solved for the elliptical tube with variable temperature. The obtained results for condensation in 100°C water vapor on the elliptical tube (e=0.9) is calculated as have been shown in Fig. 5. Temperatures of each part can be calculated according to the energy equations for different shapes. This diagram depicts the location of condensation boundary around the tube. At the top of the tube, (where the central angle is zero), the thickness of condensation boundary layer, at first, shows a little increase by the central angle and it gets thinner gradually by increasing the angle, affected by the gravitational force. Consequently, at the lower part, it cascades down the tube. Due to the nature of numerical solution, diagram of the percentage of error shows volatile amounts with huge changes at the top of the tube (in very small amounts of the central angle of the tube), and ultimately, with a very small slope, it decreases by the central angle. Local heat transfer coefficient is illustrated in Fig. 6 for each part. In addition, the numerical solution has been carried out for an elliptical tube, in which the wall temperature assumed to obey the hypothetical equation of:

$$T_w(\varphi) = T_{sat} - \overline{\Delta T}\, F_t(\varphi), \tag{30a}$$

in which

$$\begin{aligned} &\overline{\Delta T} = T_{sat} - \overline{T}_w; \quad F_t(\varphi) = 1 - A\cos\varphi, \\ &\overline{T}_w = \frac{2a}{\pi D_e}\int_0^{\pi} T_w(\varphi)[(1-e^2)/\sqrt{(1-e^2\sin^2\varphi)^3}\,]d\varphi, \\ &D_e = 2\frac{a}{\pi}\int_0^{\pi}[(1-e^2)/\sqrt{(1-e^2\sin^2\varphi)^3}\,]d\varphi, \end{aligned} \tag{30b}$$

That φ is the angle between tangential line to the tube's surface and horizontal line. A is a constant number $(0 < A < 1)$ and D_e is equivalent diameter of the ellipse. The results from the equations for calculating the heat transfer coefficient are illustrated in Fig. 7 for the elliptical tube in different boundary conditions respect to the earlier variable temperature state. It can be seen that with the increase in the thickness of the condensation boundary, the amount of heat transfer coefficient is reduced. The percentage of error is much higher in the case of variable wall temperature. Nevertheless, one can deduce that the results of numerical and theoretical solutions are very close to each other.

Fig. 8 shows the way of calculating the obtained results for the condensation of water vapor at 100 ° C around the elliptical tube (e = 0.9) with a surface temperature of 80 ° C.

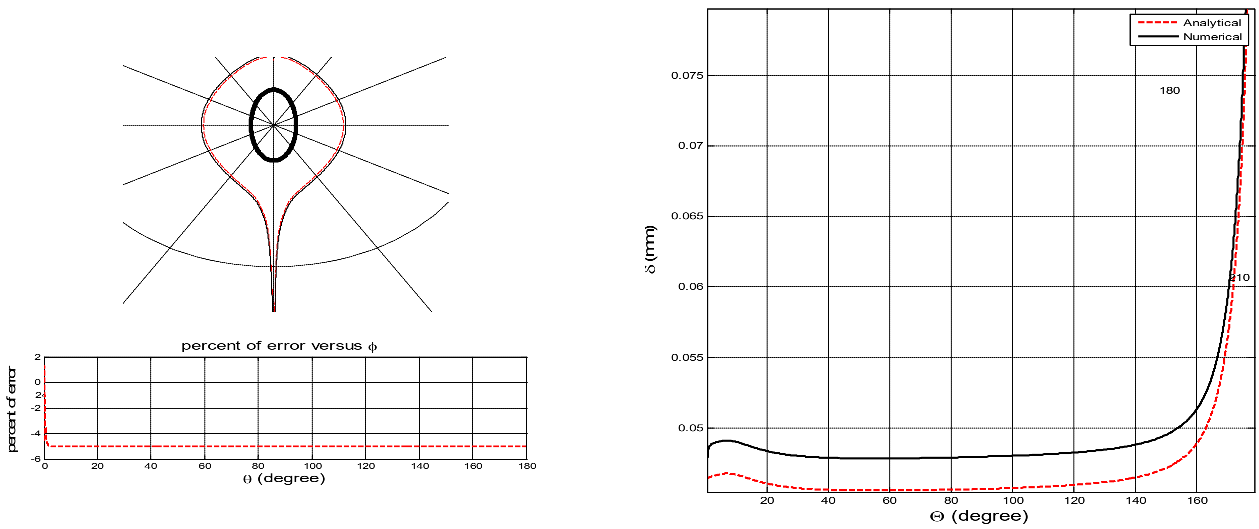

Fig. 5. Condensation Position of Horizontal Elliptic Tube in Variable Temperature Conditions

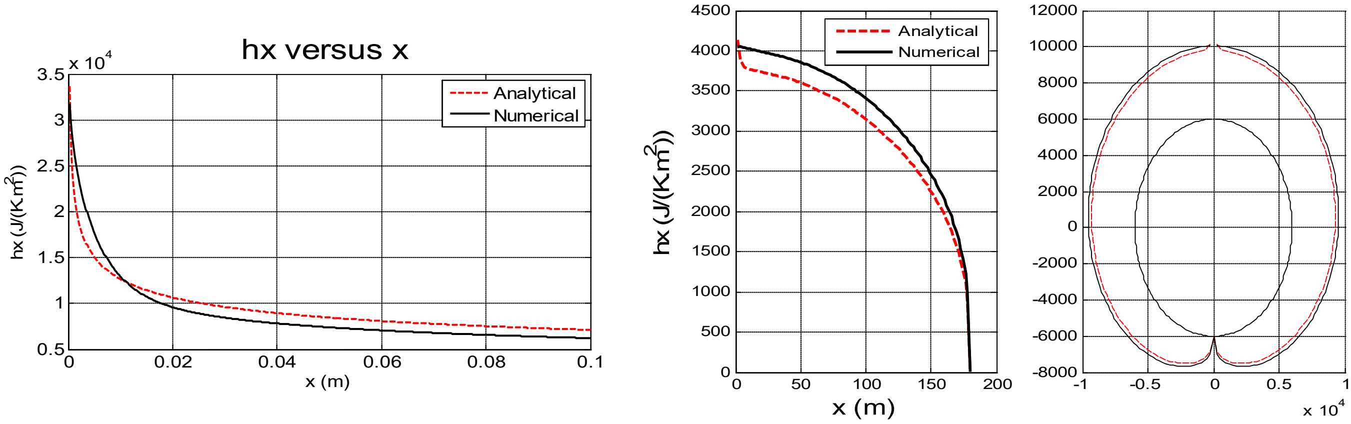

a: flat plate

b: e=0 (circle)

Fig. 6. Local Heat Transfer Coefficient Relative to the Location for the Different States with Temperature of Constant Flat Plate

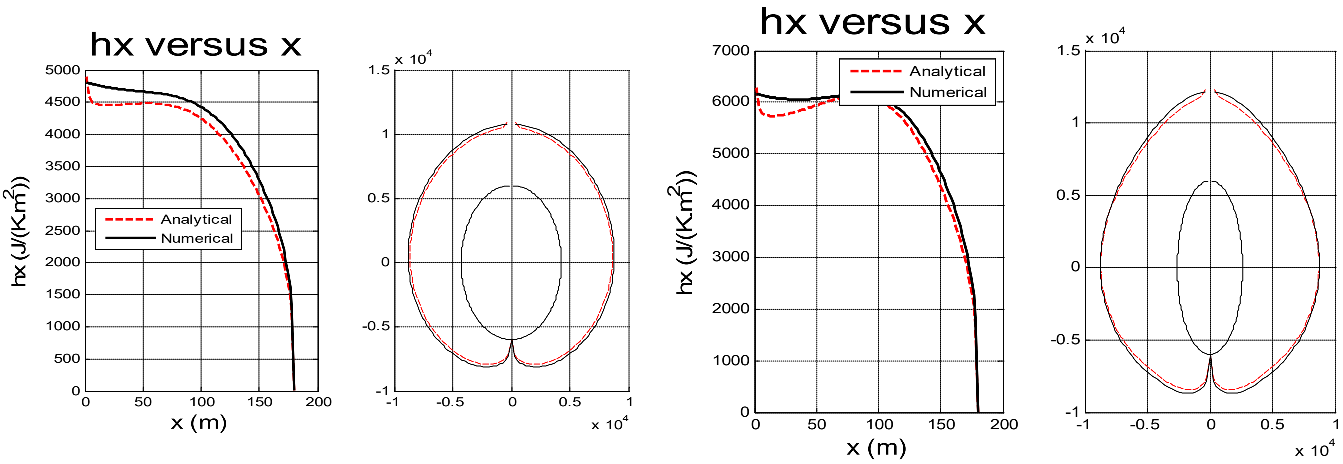

c: e=0.7

d: e=0.9

Fig. 6. Continued

In the following, entropy changes are presented for all models.

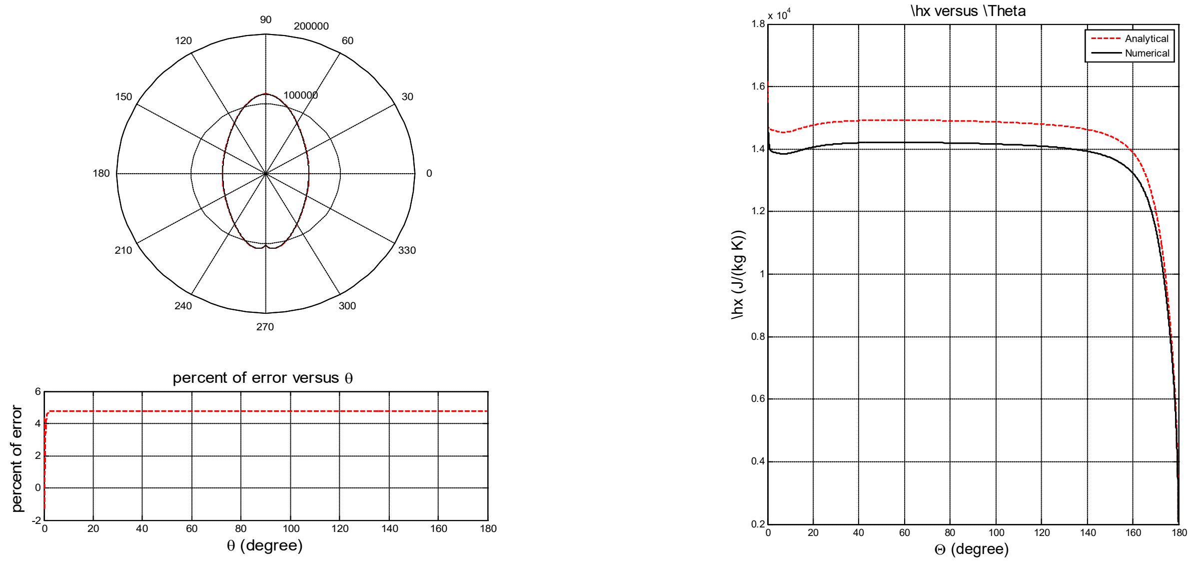

Fig. 7. Local Heat Transfer Coefficient Relative to a Variable Temperature Location

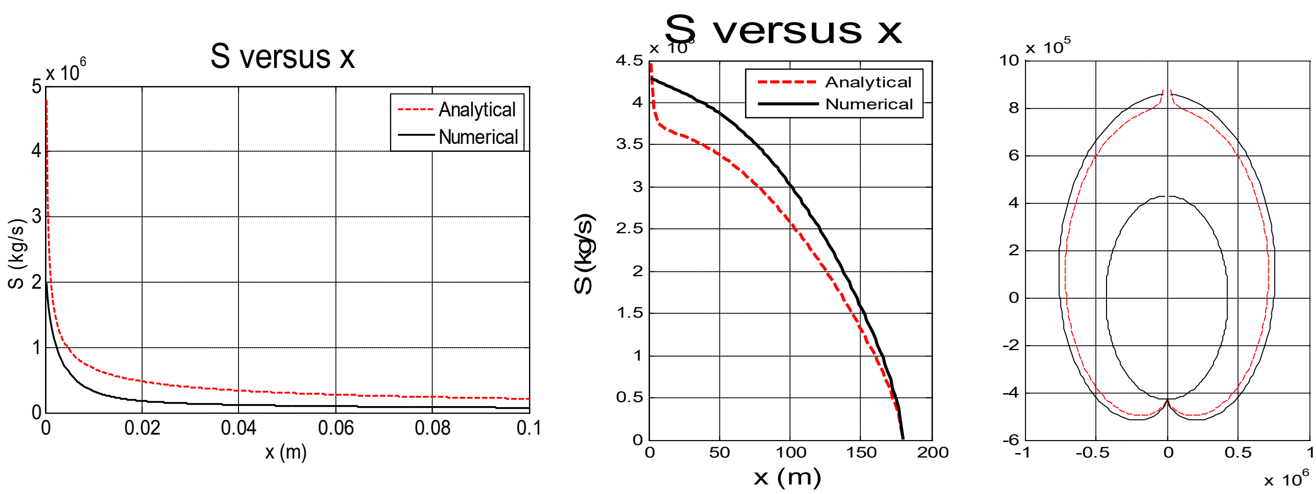

a: flat plate

b: e=0 (circle)

Fig. 8. Total Entropy Relative to Location at Constant Temperature in Different States

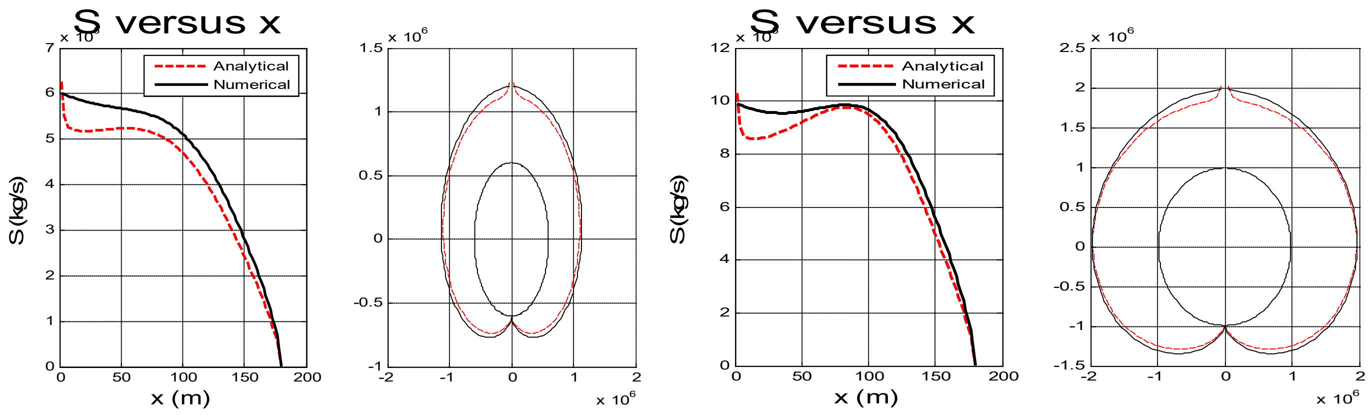

c: e=0.7

d: e=0.9

Fig. 8. Total Entropy Relative to Location at Constant Temperature in Different States

The volumetric entropy for an elliptical tube has been demonstrated in Fig. 9.

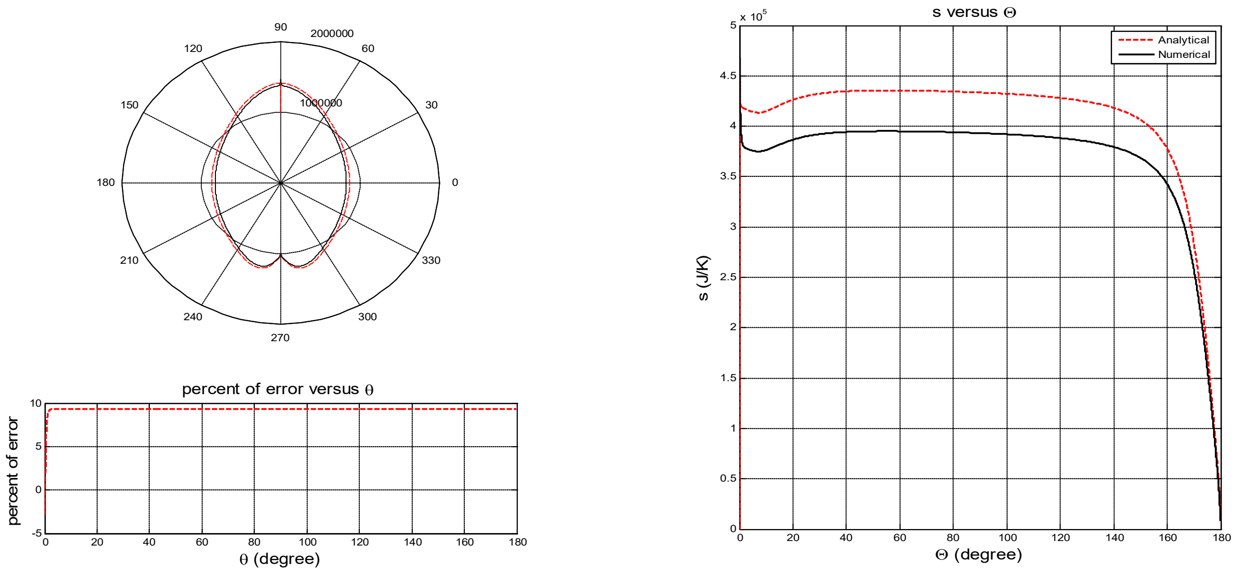

Fig. 9. Volumetric Entropy (it is constant respect to y) respect to the Location

8. Conclusion

According to the findings, it can be concluded that the analytical solution hypotheses are somewhat reasonable. These assumptions have the most error in the variable temperature problem. Diagram of error percentage is plotted for the results. The error is high on the top of ellipse, but it decreases when it goes to the bottom of the tube. This is also satisfied with the circle and the flat plate. The average error is approximately 15% in upper half, while for the lower half it is less than 10%. Of course, the error rate varies for different fields. Generally, it can be concluded that the analytical model can be used for optimization.

Conflict of Interest

The authors declared no potential conflicts of interest with respect to the research, authorship and publication of this article.

Funding

The authors received no financial support for the research, authorship and publication of this article.

References

[1] Khu, C.H., Hung, R.Y., Lin, Y.C., Yang, S.A., Second law analysis of free convection film condensation on an inclined porous elliptical tube, *International Journal of Thermal Sciences*, 50, 2011, 1333-1338.

[2] Esfahani, J.A., Modirkhazeni, M., Entropy generation of forced convection film condensation on a horizontal elliptical tube, *Comptes Rendus Mécanique*, 340, 2012, 543–551.
[3] Yang, S.A., Hsu, C.H., Free and forced convection film condensation from a horizontal elliptical tube with a vertical plate and horizontal tube as special cases, *International Journal of Heat and Fluid Flow*, 18, 1997, 567–574.
[4] Yang, S.A., Chen, C.K., Role of surface tension and ellipticity in laminar film condensation on horizontal elliptical tube, *International Journal of Heat and Mass Transfer*, 36(12), 1993, 3135–3141.
[5] Ali, A.F.M., McDonald, T.W., Laminar film condensation on horizontal elliptical cylinders: A first approximation for condensation on inclined tubes, *ASHRAE Transactions*, 83, 1977, 242–249.
[6] Bejan, A., A study of Entropy generation in fundamental convective heat transfer, *Journal of Heat Transfer*, 101, 1979, 718–725.
[7] Sahin, A.Z., Thermodynamics of laminar viscous flow through a duct subjected to constant heat flux, *Energy*, 21(12), 1996, 1179–1187.
[8] Adeyinka, O.B., Naterer, G.F., Optimization correlation for entropy production and energy availability in film condensation, *International Communications in Heat and Mass Transfer*, 31(4), 2004, 513–524.
[9] Lin, W.W., Lee, D.J., Peng, X.F., Second-law analysis of vapor condensation of FC-22 in film flows within horizontal tubes, *Journal of the Chinese Institute of Chemical Engineers*, 32, 2001, 89–94.
[10] Dung, S.C., Yang, S.A., Second law based optimization of free convection film-wise condensation on a horizontal tube, *International Communications in Heat and Mass Transfer*, 33, 2006, 636–644.
[11] Li, G.C., Yang, S.A., Thermodynamic analysis of free convection film condensation on an elliptical cylinder, *Journal of the Chinese Institute of Chemical Engineers*, 29(5), 2006, 903-908.
[12] Li, Z., Sheikholeslami, M., Jafaryar, M., Shafee, A., Chamkha, A.J., Investigation of nanofluid entropy generation in a heat exchanger with helical twisted tapes, *Journal of Molecular Liquids*, 266, 2018, 797-805.
[13] Vatanmakan, M., Lakzian, E., Mahpeykar, M.R., Investigating the entropy generation in condensing steam flow in turbine blades with volumetric heating, *Energy*, 147, 2018, 701-714.
[14] Jafarmadar, S., Azizinia, N., Razmara, N., Mobadersani, F., Thermal analysis and entropy generation of pulsating heat pipes using nanofluids, *International Journal of Applied Thermal Engineering*, 103, 2016, 356-364.
[15] Malvandi, A., Ganji, D.D., Pop, I., Laminar filmwise condensation of nanofluids over a vertical plate considering nanoparticles migration, *International Journal of Applied Thermal Engineering*, 100, 2016, 979-986.